Exploring the Circular Polarisation of Low–Frequency Solar Radio Bursts with LOFAR

Diana E. Morosan[1] · **Juska E. Räsänen[1]** · **Anshu Kumari[1]** · **Emilia K.J. Kilpua[1]** · **Mario M. Bisi[2]** · **Bartosz Dabrowski[3]** · **Andrzej Krankowski[3]** · **Jasmina Magdalenić[4]** · **Gottfried Mann[5]** · **Hanna Rothkaehl[6]** · **Christian Vocks[5]** · **Pietro Zucca[7]**

Abstract

The Sun is an active star that often produces numerous bursts of electromagnetic radiation at radio wavelengths. Low frequency radio bursts have recently been brought back to light with the advancement of novel radio interferometers. However, their polarisation properties have not yet been explored in detail, especially with the Low Frequency Array (LOFAR), due to difficulties in calibrating the data and accounting for instrumental leakage. Here, using a unique method to correct the polarisation observations, we explore the circular polarisation of different sub-types of solar type III radio bursts and a type I noise storm observed with LOFAR, which occurred during March–April 2019. We analysed six individual radio bursts from two different dates. We present the first Stokes V low frequency images of the Sun with LOFAR in tied-array mode observations. We find that the degree of circular polarisation for each of the selected bursts increases with frequency for fundamental emission, while this trend is either not clear or absent for harmonic emission. The type III bursts studied, that are part of a long–lasting type III storm, can have different senses of circular polarisation, occur at different locations and have different propagation directions. This indicates that the type III bursts forming a classical type III storm do not necessarily have a common origin, but instead they indicate the existence of multiple, possibly unrelated acceleration processes originating from solar minimum active regions.

✉ D.E. Morosan
  diana.morosan@helsinki.fi

1 Department of Physics, University of Helsinki, P.O. Box 64, 00014 Helsinki, Finland

2 RAL Space, United Kingdom Research and Innovation – Science and Technology Facilities Council – Rutherford Appleton Laboratory, Harwell Campus, Oxfordshire OX11 0QX, UK

3 Space Radio-Diagnostics Research Centre, University of Warmia and Mazury, Olsztyn, Poland

4 Solar–Terrestrial Centre of Excellence—SIDC, Royal Observatory of Belgium, 1180 Brussels, Belgium

5 Leibniz–Institut für Astrophysik Potsdam (AIP), An der Sternwarte 16, 14482, Potsdam, Germany

6 Space Research Center, Polish Academy of Sciences, 00-716, Warsaw, Poland

7 ASTRON, The Netherlands Institute for Radio Astronomy, Oude Hoogeveensedijk 4, 7991 PD Dwingeloo, The Netherlands

1. Introduction

Bursts of electromagnetic radiation at radio wavelengths are a common phenomenon on the Sun. They can occur during large solar explosions and eruptions, namely flares and coronal mass ejections (CMEs), and also in their absence. These bursts are classified into five main types: type I – V (Wild, 1963). Type I and type III radio bursts usually dominate the observations of solar activity at meter wavelengths in the absence of large eruptive events.

Type III bursts are rapidly varying bursts of radiation at meter wavelengths that show a fast drift in the dynamic spectra from high to low frequencies and last for a few seconds (e.g. Wild, 1950; Reid and Ratcliffe, 2014; Morosan et al., 2014; McCauley, Cairns, and Morgan, 2018; Mugundhan et al., 2018b). Type III bursts are often associated with flaring activity, however they frequently occur in the absence of solar flares or other eruptive events (Dulk, 1985). They have been observed over a wide frequency range from GHz (e.g. Ma et al., 2012) to kHz (e.g Krupar et al., 2018), though most frequently, they occur at frequencies < 150 MHz (Saint-Hilaire, Vilmer, and Kerdraon, 2013). Type III bursts represent the radio signature of electron beams travelling through the corona and into interplanetary space along open and quasi-open magnetic field lines (Ginzburg and Zhelezniakov, 1958; Lin, 1974; Reid and Ratcliffe, 2014). Some sub-types of type III bursts, such as J- or U-bursts, indicate the presence of electron beams travelling along closed magnetic loops (Maxwell and Swarup, 1958; Stone and Fainberg, 1971; Morosan et al., 2017; Reid and Kontar, 2017). It is commonly believed that following acceleration, faster electrons outpace the slower ones to produce a bump-on-tail instability in their velocity distribution. This generates Langmuir (plasma) waves, which are then converted into radio waves at the plasma frequency, f_p, and its harmonic, $2f_p$ (Bastian, Benz, and Gary, 1998), where the plasma frequency is defined as $f_p \sim C\sqrt{(n_e)}$, with n_e being the electron number density and C is a constant.

Type I bursts are non-thermal radio emissions generally associated with active regions (McCready, Pawsey, and Payne-Scott, 1947; Wild, 1951; Swarup, Stone, and Maxwell, 1960; Melrose, 1975). They consist of short duration narrow–band bursts which can last for a few seconds to a few minutes (Takakura, 1963; Ellis, 1969; Mugundhan et al., 2018a). These narrow-band bursts form a continuum emission known as a noise storm, which lasts from a few hours to a few days (Elgarøy, 1977; Thejappa and Kundu, 1991; Kathiravan, Ramesh, and Nataraj, 2007). Type I noise storms/bursts are often found to be highly circularly polarised (see for example, Payne-Scott (1949), Ramesh et al. (2013) and references therein). These bursts occur over a wide frequency range of $\sim 30 - 200$ MHz (Elgarøy, 1977; Spicer, Benz, and Huba, 1982; Yu et al., 2019), with a few exceptions.

While the spectroscopic and spatial properties of type III and type I bursts have been studied in great detail (e.g. Wild, 1967; Reiner, Fainberg, and Stone, 1995; Saint-Hilaire, Vilmer, and Kerdraon, 2013; Morosan et al., 2014; Ramesh, Mugundhan, and Prabhu, 2020; Elgarøy, 1977; Yu et al., 2019), the circular polarisation of low frequency solar radio bursts is still poorly documented due to the previous unavailability of spectropolarimetric observations, except for a few instances, see for example Payne-Scott (1949), Elgarøy (1977), Ramesh et al. (2013), Mugundhan et al. (2018b). Early observations of type III radio bursts have shown that the fundamental emission is highly circularly polarised, while the harmonic has a low degree of circular polarisation or is unpolarised (Dulk and Suzuki, 1980). Type I noise storms are also highly polarised (up to $\sim 100\%$) and are believed to be generated

at the fundamental plasma frequency (Benz and Zolliker, 1985; Ramesh et al., 2013). Recent studies with the Murchison Widefield Array (MWA; Tingay et al., 2013) produced spectropolarimetric images of the radio Sun at low frequencies in the range $80 - 240$ MHz (McCauley et al., 2019; Rahman, Cairns, and McCauley, 2020). Type III radio bursts have been studied in detail with the MWA, and Rahman, Cairns, and McCauley (2020) found that the degree of circular polarisation increases with frequency for fundamental emission type III bursts. However, no such studies have been carried out yet with LOFAR, which is capable of observations at even lower frequencies (down to 20 MHz) compared to the MWA (down to 80 MHz).

Polarisation observations of solar radio bursts are still difficult to carry out due to the complexity in the calibration of polarised signals that are in part due to the lack of circularly polarised calibration sources and in part due to instrumental effects. With the advancement of novel radio instrumentation such as the Low Frequency Array (LOFAR; van Haarlem et al., 2013) and the MWA, spectropolarimetric imaging observations are now possible in the low frequency radio domain with a high temporal and frequency resolution. However, careful investigation of instrumental effects and signal leakage must be taken into account.

In this paper, we present for the first time a method for obtaining polarization information of solar radio bursts with LOFAR which takes into account instrumental leakage. We present the first spectropolarimetric and imaging observations with LOFAR of a few subtypes of type III bursts and a type I noise storm. In Section 2 we give an overview of the LOFAR instrument, the observational mode used, and the data processing methods. In Section 3 we present our results, which are further discussed in Section 4.

2. Observations and Data Analysis

2.1. LOFAR Full Stokes Observations

LOFAR is a next-generation radio telescope consisting of thousands of dipole antennas forming individual stations across Europe (van Haarlem et al., 2013). Here we use tied-array beam observations of the Sun (Stappers et al., 2011; van Haarlem et al., 2013) carried out during an observing campaign in March–April 2019. These observations were recorded in the frequency range $20 - 80$ MHz, using the Low Band Antennas (LBAs) from LOFAR's core, which is located in the Netherlands. We used a total of 126 beams that are pointing in a concentric pattern around the Sun to sample different locations. Due to the nature of the observations, and in order to accommodate the interferometric mode simultaneously with the tied-array beam observations, only a limited selection of frequency subbands were available for the beam-formed observations. The tied-array beam observations contain a total of 60 subbands distributed over $20 - 80$ MHz. Each subband has a bandwidth of 195.3 kHz and is further divided into 16 frequency channels. The frequency resolution of each subband is 12.2 kHz. The frequency subbands are not uniformly distributed in the $20 - 80$ MHz frequency range, therefore the frequency coverage is not continuous. However, due to the large number of subbands used, we can obtain an almost complete picture of the time–frequency evolution of individual radio bursts.

The tied-array beam observations are recorded as dynamic spectra in Stokes I, Q, U and V for each of the 126 beams. The dynamic spectra are then calibrated using a separate beam pointing at an external calibrator throughout the observation. In this study, we used Taurus A as a calibrator. Stokes I, Q, U and V are given by the following relations (Hales, 2017;
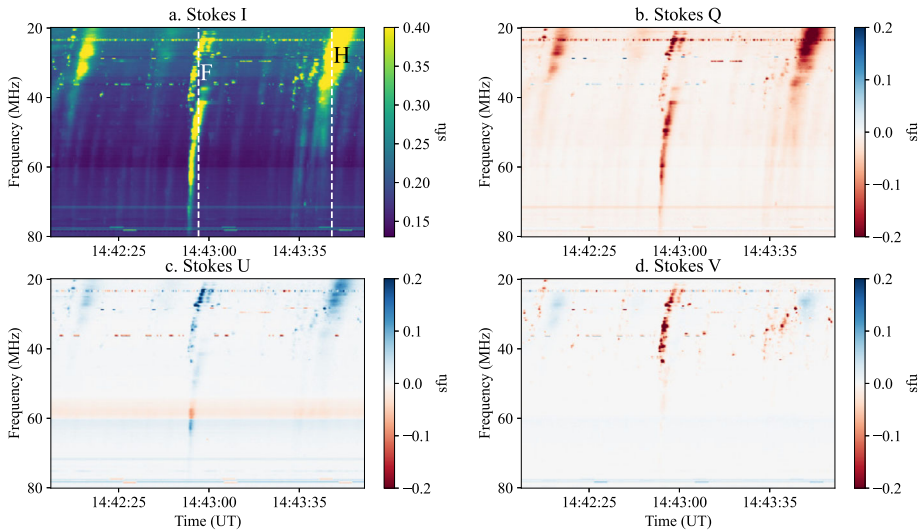
Figure 1 Dynamic spectrum showing a number of type III radio bursts including both fundamental and harmonic emissions in Stokes I (**a**), Q (**b**), U (**c**) and V (**d**).

Robishaw and Heiles, 2021):

$$I = |A_x|^2 + |A_y|^2 \tag{1}$$

$$Q = |A_x|^2 - |A_y|^2 \tag{2}$$

$$U = 2A_x A_y \cos\delta \tag{3}$$

$$V = 2A_x A_y \sin\delta, \tag{4}$$

where A_x and A_y are the dipole voltages of each of the two orthogonal LBA antennas and δ is the phase difference. For circular polarisation, $\delta = \pm\pi/2$.

The dynamic spectrum beams are then used to make tied-array images of the Sun for each Stokes component using the methods of Morosan et al. (2014, 2015). This is done by interpolating between the intensity of emission of each individual beam at a given time and frequency. The images made using the calibrated dynamic spectra show flux density values in solar flux units (sfu, where 1 sfu = 10^{-22} W m^2 Hz^{-1}) in both Stokes I and V. Each image is averaged over a time period of 0.5 s and over one full frequency subband. An example of a calibrated dynamic spectrum as well as tied-array images examples in Stokes I, Q, U and V (before correcting for instrumental leakage) are shown in Figures 1 – 3 for all Stokes components.

At low radio frequencies (< 100 MHz), the distance between the source and the observer is so large that the linear polarisation when averaged over an observing frequency band is expected to cancel out due to the Faraday rotation of the plane (Grognard and McLean, 1973; Sasikumar Raja et al., 2013). Thus, the signals in Stokes Q and U (linearly polarised) is cancelled out over a certain size bandwidth. Therefore, the resulting low frequency solar radio emission is, in theory, only observed in Stokes I and V (see for example Sastry, 2009; Kumari et al., 2017a, 2019). However, some signal is often found in Stokes Q and U, which
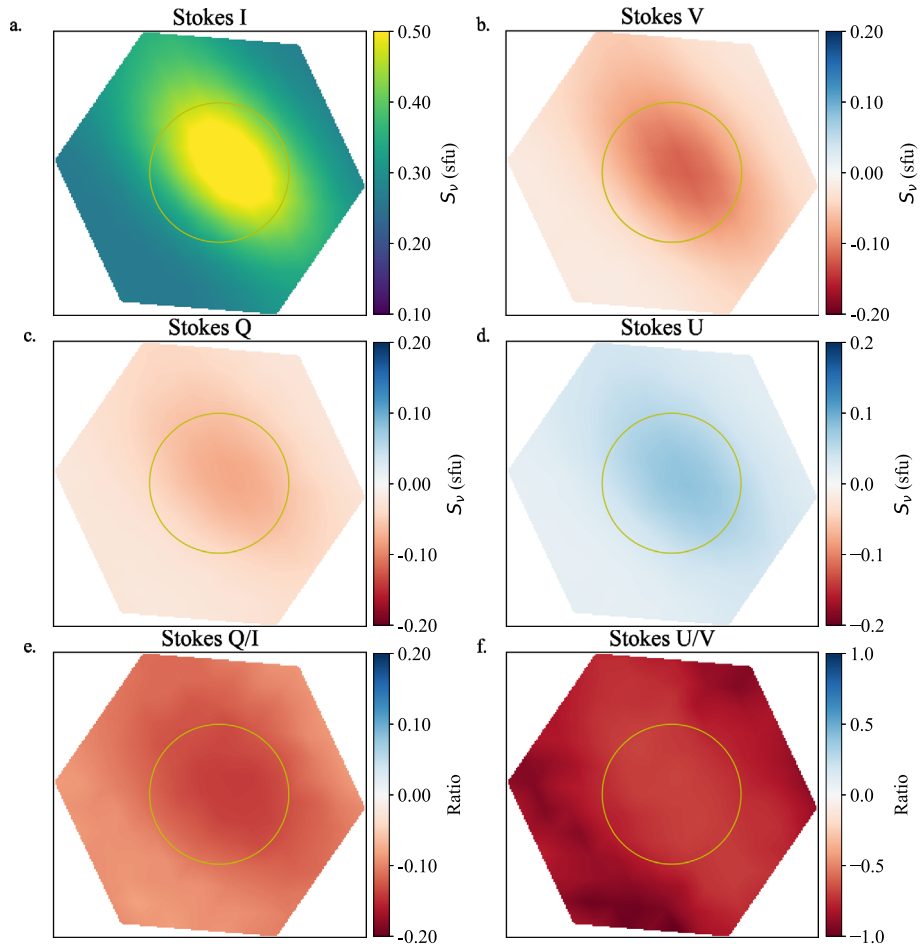
Figure 2 LOFAR tied-array images of the type III radio burst, denoted by the first dashed line in Figure 1 at 14:42:56 UT and a frequency of 27.4 MHz. Panels **a** – **d** show the Stokes I, V, Q and U images, while the last two panels **e** – **f** show the ratios Q/I and U/V used to investigate leakage. In this case, the signal in Stokes U is smaller than that in Stokes V.

is most likely a leakage from Stokes I and Stokes V due to the cross-correlation of the dipole antenna voltages (Ramesh et al., 2008; Kumari et al., 2017b; Mugundhan et al., 2018a; Kumari et al., 2021). This leakage is difficult to estimate due to the unavailability of polarised calibrators in the sky.

The tied-array beams mode offers a unique possibility of quantifying the extent of polarisation leakage in Stokes Q and U to obtain more accurate estimates of the signals in Stokes I and V. The signal can be analysed in all 126 individual beams, both on and off source, to determine the extent of the leakage. However, this is done under the assumption that no residual linearly polarised signal is detected. A dynamic spectrum of a few type III radio bursts is shown in Figure 1 in Stokes I (a), Q (b), U (c) and V (d). While there is a clear signal in Stokes V which shows the circular polarisation of some of these type III bursts, a significant signal is also observed in Stokes Q and U. For the fundamental type III radio burst (labelled as F in Figure 1a), we observe a significant signal in Stokes V and some weaker
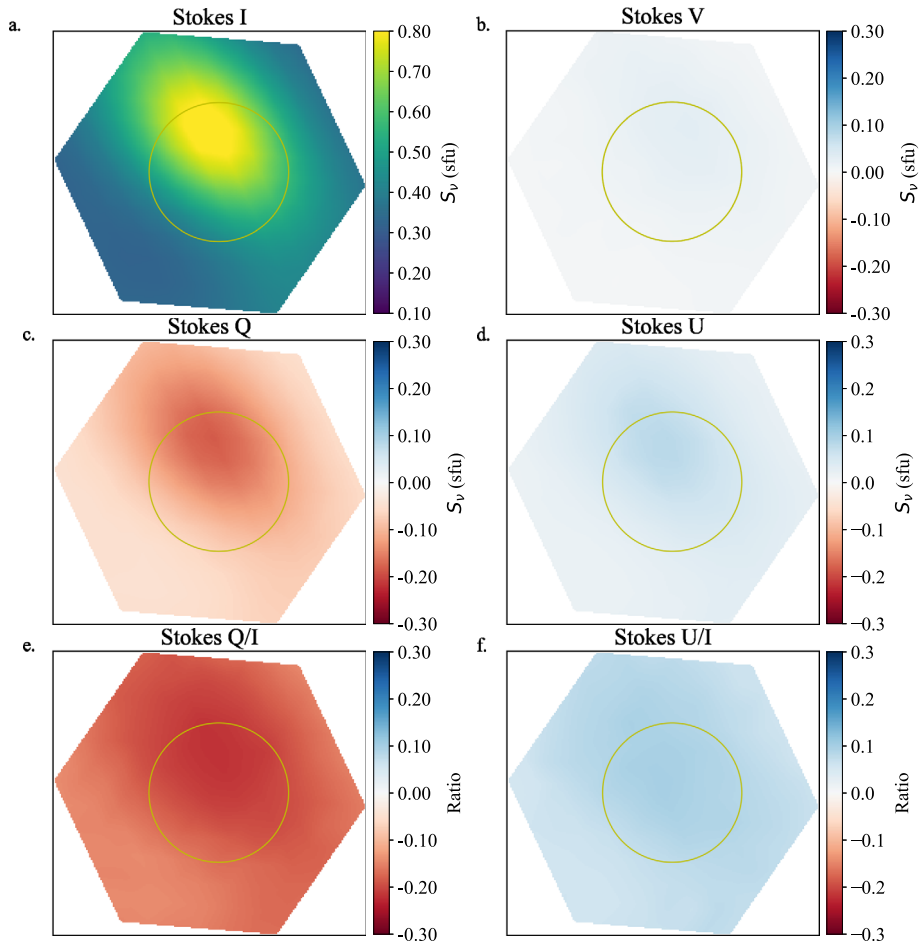
Figure 3 LOFAR tied-array images of the type III radio burst denoted by the second dashed line in Figure 1 at 14:43:47 UT and a frequency of 27 MHz. Panels **a – d** show the Stokes I, V, Q and U images, while the last two panels **e – f** show the ratios Q/I and U/I used to investigate leakage. In this case, there is no circularly polarised signal and thus the signal in Stokes U is greater than in Stokes V.

signal in Stokes U, which would indicate a leakage from Stokes V to Stokes U. However, for the radio bursts that are weak in Stokes V, which are mostly harmonic emissions (labelled as H in Figure 1a), the signal in Stokes U is greater than in Stokes V. All radio bursts show a signal in Stokes Q, which indicates leakage from Stokes I into Q.

In order to quantify the amount of leakage in Stokes Q and U and determine the origin of the additional signal in Stokes U when there is no signal in Stokes V, we investigated tied-array images in all Stokes components. Thus, we can estimate the polarisation leakage on and off source (in our case in radio burst beams and quiet beams, respectively). We investigated two cases where the signal in Stokes U is smaller than that in Stokes V (Figure 2) and the signal in Stokes U is greater than that in Stokes V (Figure 3). Then, by taking ratios U/I, U/V, Q/I, we can determine the percentage of leakage from I and V into either Stokes Q and U. When there is a signal in Stokes V (Figure 2), there is on-source leakage

from Stokes V to U, however, in the beams pointing off-source, the ratio U/V > 1 (Figure 2f) which indicates that not all signal leakage is from Stokes V. When there is no significant signal in Stokes V (Figure 3b) and thus U > V (Figure 3d), there is signal in U both on- and off-source, which is consistent with leakage from Stokes I, since the ratio U/I (Figure 3f) is roughly uniform across all beams and shows less variation compared to the ratio Q/I. There is also continuous leakage from Stokes I into Stokes Q both on- and off-source. We did not find any clear evidence of leakage of Stokes V into Q. This is hard to identify as Stokes I is always present and dominates the emission observed in Stokes Q.

The Stokes I spectra (I_{corr}) are thus corrected in the following way:

$$I_{corr} = I + F_Q I + F_U I, \tag{5}$$

where F_Q and F_U represent the fraction of Stokes I leakage into Stokes Q and U, respectively. The leakage in Stokes U is approximately uniform and a value of $\sim$5% was selected which represents the off-source leakage. The signal in Stokes Q can vary with subband and on- and off-source position and is in the range $5-30\%$ of the signal in Stokes I. We selected the median value of F_Q for each subband to correct Stokes I.

The Stokes V spectra (V_{corr}) are corrected using the following relation, to include the signal leakage in U back into the Stokes V component, as follows:

$$V_{corr} = \frac{V}{|V|}\sqrt{V^2 + (|U| - F_U I)^2}. \tag{6}$$

Here the ratio $V/|V|$ is used to preserve the sign of V, since correcting Stokes V requires a sum of squares method. The sign of V is also strongly dependent on the sign of δ, unlike Stokes U. The square root term of the equation adds back the Stokes V signal spilled into Stokes U after Stokes U has been corrected for the leakage from Stokes I. The leakage from I into U is small ($F_U = \sim$5%) and is subtracted from the absolute value of U so that it is not added into Stokes V. The leakage of V into U is in the range of $5-30\%$ depending on on- and off-source location and the subband.

2.2. Radio Bursts Observations

During the LOFAR observing campaign in March–April 2019, we observed a long-lasting type III storm, including numerous sub-types of type III bursts, and also a long-lasting type I noise storm. The observed bursts are not associated with a particular solar flare, however a few C-class flares occurred at the end of March 2019 and only some B-class flares in the beginning of April 2019, when the bursts presented in this study were observed.

In this study, we investigate the circular polarisation and spatial location of six individual radio bursts outlined in Table 1, in order to demonstrate LOFAR's spectropolarimetric capabilities. For each burst, we extracted the time series averaged over a full subband in all Stokes components. We then used Stokes I, Q, U and V to obtain the degree of circular polarisation of each burst. Stokes V is used to obtain information on the sense of circular polarisation of each burst. Figure 4 shows the dynamic spectra for these individual bursts along with the time series of the subband-averaged Stokes components. The non-uniform subband coverage often results in a not so smooth transition between the frequency channels, which can make the harmonic components of type III bursts appear patchy in a similar way to the fundamental emission (see, for example, the harmonic emission intersected by the first white dashed vertical line in Figure 1a).

Table 1 Radio bursts observed with LOFAR and their properties including date and time, type (FH=Fundamental–Harmonic), maximum degree of circular polarisation (dcp) estimated in Section 3.3, and sense of circular polarisation.

Burst	Date and start time (UT)	Type	Maximum dcp	Sense
1	2019-03-21 14:22:59	FH Type III Pair	65% (F)/15% (H)	−V
2	2019-03-21 14:33:27	Stria chain	45% (F)	−V
3	2019-03-21 14:42:50	FH Type III Pair	70% (F)/20% (H)	−V
4	2019-03-21 14:44:42	J-burst Pair	15% (H)	+V
5	2019-04-08 12:20:00	Type I	100% (F)	−V
6	2019-04-08 12:58:43	FH Type III Pair	50% (F)/20% (H)	−V

3. Results

3.1. Radio Bursts and Their Circular Polarisation

The radio bursts outlined in Table 1 were studied in detail to obtain their degree of circular polarisation (dcp) and the sense of circular polarisation (determined using the sign of V). Table 1 also contains a summary of their properties such as date and start time, type, maximum dcp and sense of circular polarisation. The radio bursts include sub-types of type III radio bursts (such as stria bursts and J-bursts) and a type I noise storm (Burst 5). Bursts 1 – 4 were observed on 21 March 2019 and Bursts 5 – 6 on 8 April 2019. The spectral and polarisation properties of these bursts are discussed here:

Burst 1 consists of a type III fundamental–harmonic (FH) pair observed on 21 March 2019 which started at 14:22:59 UT (Figure 4a). The FH components extend over the entire frequency range of the observation. An example of a time series averaged over one subband extending from 31.34 – 31.53 MHz and a centre frequency of 31.44 MHz is shown in the bottom panel of Figure 4a. The time series reveals that the fundamental emission (which corresponds to the stria burst occurring before 14:23 UT) appears highly polarised, i.e. the Stokes V intensity (red solid line) is comparable to that of Stokes I (blue solid line). On the other hand, the harmonic (which corresponds to the smoother burst after 14:23 UT) appears almost unpolarised (Stokes V∼0), which agrees with previous findings (e.g. Dulk and Suzuki, 1980). This is consistent for all individual subbands in the 20 – 80 MHz range. The sign of Stokes V is negative. There is however a small signal in Stokes U (green solid line in Figure 4a) which is used to correct the Stokes V signal, and a significant signal in Stokes Q used to correct the Stokes I signal.

Burst 2 represents a chain of stria bursts (the intermittent structures usually forming a fundamental type III burst) observed on 21 March 2019 starting at 14:33:27 UT (Figure 4b). The stria chain extends from 20 – 50 MHz. The stria bursts usually represent emission forming a fundamental type III burst and are moderately circularly polarised (Figure 4b), which remains consistent throughout each subband containing the bursts. The sign of Stokes V is negative.

Burst 3 consists of another type III FH pair observed on 21 March 2019 starting at 14:42:50 UT (Figure 2c). In this case, the fundamental component is also highly circularly polarised, while the harmonic is almost unpolarised. The sign of Stokes V is negative similar to the previous FH type III burst discussed.

Burst 4 consists of a pair of J-bursts observed on 21 March 2019, which started at 14:44:42 UT (Figure 2d). The J-bursts represent harmonic emission that is weakly circularly polarised. The sign of Stokes V is positive, which is opposite to the other bursts studied
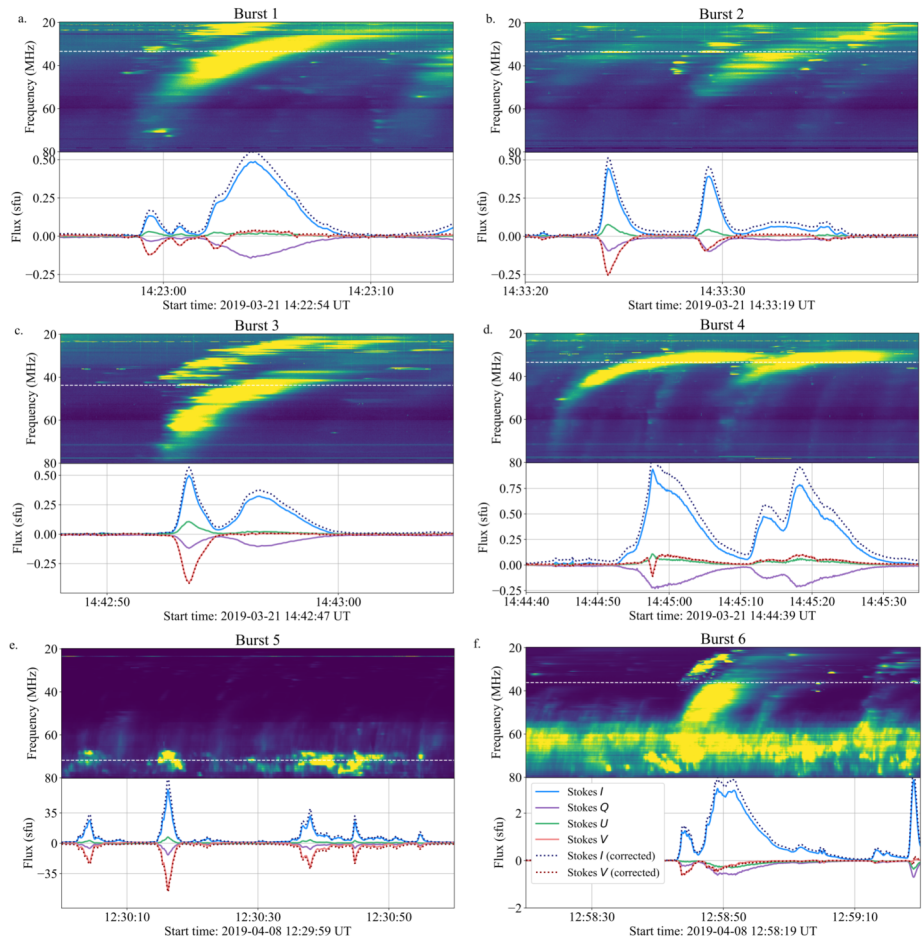
Figure 4 Dynamic spectra in Stokes I and time series for Stokes I (blue), Q (purple), U (green), V (red), I corrected (dark blue dotted) and V corrected (dark red dotted) for the bursts outlined in Table 1. For each burst, the time series is averaged over the subband outlined by the white dashed lines in the dynamic spectra with a center a frequency of 31 MHz (**a**, **b**, **d**, and **f**), 43 MHz (**c**) and 70 MHz (**f**).

here. Since J-burst emitting electrons propagate along closed magnetic-field lines, it is likely that they propagate along different magnetic field lines to the other bursts observed on 21 March 2019 that are expected to propagate along the open field instead. Thus, they can have a different sense of circular polarisation than the other bursts.

Burst 5 consists of type I bursts forming a long-lasting type I noise storm that started on 8 April 2019 at ∼12:30 UT (Figure 2e). The type I bursts are strongly circularly polarised and occur simultaneously with fainter type III radio bursts. The sign of Stokes V is negative. Type I emission is only observed in the 60 – 80 MHz frequency range.

Burst 6 consists of a type III FH pair observed on 4 April 2019 starting at 12:58:43 UT (Figure 2f), during the type I noise storm. This type III was selected as it has a similar flux density value to the type I noise storm and also occurs on a background of fainter type III activity. The fundamental component is also highly circularly polarised, while the harmonic
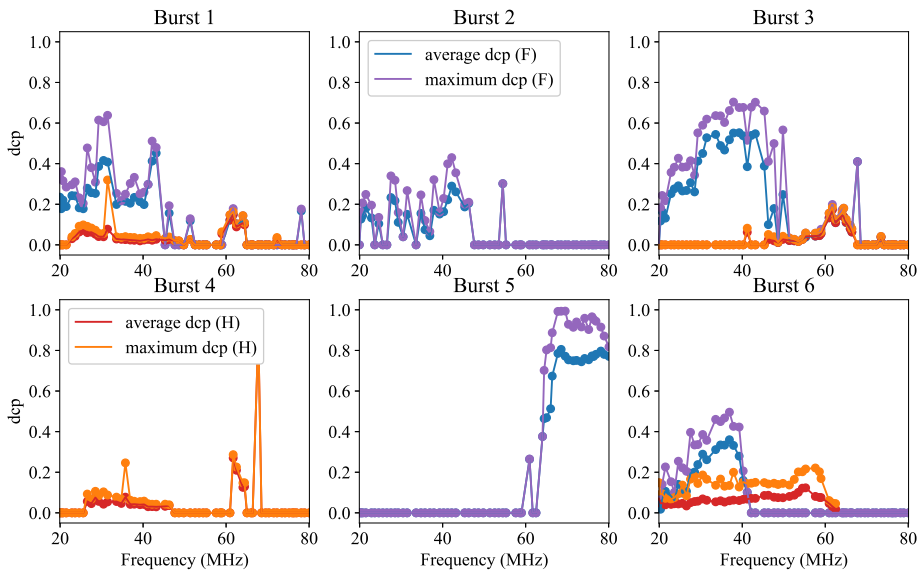
Figure 5 Degree of circular polarisation (dcp) of the bursts outlined in Table 1 as a function of frequency. The red, orange, blue and purple lines represent the average and maximum dcp of the harmonic (H) and fundamental (F) components of the bursts discussed here, respectively.

is weakly polarised. The sign of Stokes V is negative, same as with the type I noise storm. This burst has a higher flux density than the other FH bursts reported here.

3.2. Degree of Circular Polarisation of Observed Bursts

For each of the bursts outlined in the previous section, we computed the degree of circular polarisation (dcp) as a function of frequency (Figure 3). The degree of circular polarisation (dcp) is obtained as,

$$\text{dcp} = \frac{V_{corr}}{I_{corr}}. \tag{7}$$

The dynamic spectra and radio images can now be used to extract simultaneously the degree of circular polarisation, the location and the trajectory of the radio emission that are presented in the following sections. The dcp was computed by averaging the data over a time period of 0.5 s and over a full frequency subband. The maximum dcp is summarised in Table 1. The panels in Figure 5 show the average and maximum dcp for each subband in the case of each burst. The average and maximum dcp were computed for each subband over a time range comprising of the entire duration of each burst.

   We found that the dcp for type III fundamental emission is large (40 – 75%) while the observed harmonic emission is weakly polarised (up to 25%). In the case of the bursts studied here, the dcp is higher than the average dcp of type III bursts recorded by Dulk and Suzuki (1980) in the range of 24 – 220 MHz, but comparable to values reported in more recent studies by Rahman, Cairns, and McCauley (2020). The type I storm is also highly circularly polarised with dcp values reaching 100%, in agreement with previous studies (e.g. Dulk and Nelson, 1973). We also found a clear trend of the dcp increasing with frequency, in the case

of fundamental emissions, consistent with the findings of Rahman, Cairns, and McCauley (2020) with the MWA. This is also seen in the case of harmonic emission for Bursts 3 and 6, however, an opposite trend is seen for Bursts 1 and 4.

In the case of Bursts 1, 2 and 5, there appears to be fluctuations in both average and maximum dcp values. However, due to the uneven distribution of subbands in this observational setup, fine-structured bursts, especially striae, can be abruptly cut off. These fluctuations arise due to the discontinuous frequency coverage. In the case of the fundamental emission for Bursts 1 and 2, fluctuations may also arise due to averaging of the signal over the individual striae or the gap between the striae.

3.3. Locations of Observed Bursts and Their Sense of Circular Polarisation

The radio centroids of the observed bursts were extracted from the tied-array images by fitting a two-dimensional elliptical Gaussian to the radio sources (for more information, see the methods described in Morosan et al. 2019). The radio centroids are shown in the panels of Figure 6 overlaid on top of extreme ultraviolet images from the Sun-Watcher with Active Pixel System and Image Processing (SWAP; Seaton et al., 2013) instrument onboard the Project for On Board Autonomy 2 (PROBA2; Santandrea et al., 2013) spacecraft. The centroids are obtained from images at different frequencies spread over the spectral extent of each burst to show the propagation direction of the bursts. Burst 1 centroids are at frequencies of $29-47$ MHz, Burst 2 at $20-41$ MHz, Burst 3 at $24-43$ MHz, Burst 4 at $30-43$ MHz, Burst 5 at $24-55$ MHz, and Burst 6 at frequencies of $61-76$ MHz.

The location of the centroids show that the radio bursts that occurred on 21 March 2019 have different propagation directions, which is in agreement with the wide variety of dcp values and different senses of circular polarisation observed. It is also interesting to note that Burst 1 and Burst 3, on 21 Mach 2019 that are both of FH type III bursts, originate in different locations and propagate in opposite directions, as seen in Figure 6. The FH pair in Burst 1 propagates radially outwards, while the FH pair in Burst 3 propagates inwards across the solar disk. The J-bursts (Burst 4) propagate towards the north pole, most likely along close magnetic loops, with one footpoint in one of the active regions present in the western hemisphere. A scenario that could explain these propagation directions is open or quasi-open magnetic-field lines branching outwards as a fan and electron beams can then escape along these different field lines. All the bursts appear to originate from the solar hemisphere, which contains active regions, and most likely originate due to processes in or near the two active regions present in the western hemisphere.

The centroids of the bursts on 8 April 2019 (both type I and type III) have smaller uncertainties due to the much larger flux densities of these bursts compared to the background emission (for more details on estimating the centroid uncertainties please see Morosan et al., 2019). The overlap of various frequencies at the same location indicates that despite being limb events, plane-of-sky projection effects are significant in the case of the these bursts. The type III, in particular, is propagating out of the plane-of-sky towards or away from the observer. In this case, it is more likely that these bursts are propagating away from the observer, since the active region is just rotating on the visible solar disc and the magnetic-field lines are mostly connected to regions that are still behind the limb.

4. Discussion and Conclusion

Type III and type I radio bursts are emitted by plasma radiation in the solar corona. This emission originates as a result of Langmuir (plasma) waves that are generated by accelerated

a. SWAP 174 Å 2019-03-21 14:33 UT   b. SWAP 174 Å 2019-04-08 12:31 UT
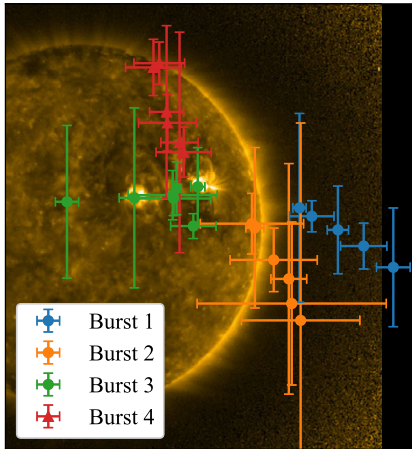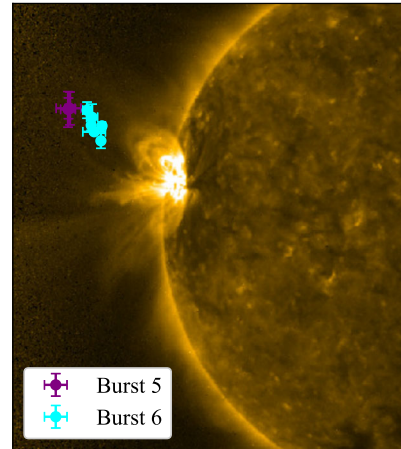
Figure 6 Radio burst centroids obtained from tied-array images of the Sun. (**a**) Centroids of the type III bursts (Bursts 1 – 4) observed on 21 March 2019 overlaid on a PROBA-2/SWAP extreme-ultraviolet image of the Sun. (**b**) Centroids of the type I and type III bursts (Bursts 5 and 6, respectively) observed on 8 April 2019 overlaid on a PROBA-2/SWAP extreme-ultraviolet image of the Sun. The centroids were obtained from images at several frequencies spread over the spectral extent of each burst. Burst 1 centroids are at frequencies of 29 – 47 MHz, Burst 2 at 20 – 41 MHz, Burst 3 at 24 – 43 MHz, Burst 4 at 30 – 43 MHz, Burst 5 at 24 – 55 MHz and Burst 6 at frequencies of 61 – 76 MHz.

electron beams propagating through the coronal plasma (Stewart and Labrum, 1972; Suzuki and Dulk, 1985). For Langmuir waves travelling parallel or anti-parallel to the magnetic field, the polarisation is in the sense of the ordinary (o-) mode (Dulk et al., 1976; Dulk and Suzuki, 1980). The o-mode is the only mode that can theoretically propagate through the coronal plasma to produce fundamental plasma emission, since the x-mode is blocked (Melrose, 2009). The fundamental radiation is then expected to be up to 100% polarised (Melrose and Sy, 1972). Type III and type I bursts have also been often reported as o-mode radiation (e.g. Dulk and Suzuki, 1980; Dulk and Nelson, 1973).

In our study, the FH type III bursts observed on 21 March 2019 (Burst 1 and Burst 3) show fundamental emission that is highly circularly polarised (65% and 75%, respectively). The fundamental emission is expected to be up to 100% polarised, however, previous studies reported that type III bursts show clear depolarisation effects, since the observed dcp ≪ 100% (Dulk and Suzuki, 1980; Mercier, 1990; Rahman, Cairns, and McCauley, 2020). On the other hand, observations of type I storms have found that they are up to 100% circularly polarised (e.g. Kai, Melrose, and Suzuki, 1985; Mugundhan et al., 2018a). The type I burst observed here, Burst 5, is indeed up to 100% circularly polarised. The main theory attributed to the depolarisation of type III bursts is due to scattering effects of radio waves as they propagate through the coronal plasma (Robinson, 1983; Melrose, 1989; Rahman, Cairns, and McCauley, 2020). In the case of Bursts 1 and 3 observed here, we report very high dcp values for the fundamental emission, especially during the burst onset at higher frequencies, however, the highest dcp value is 75% similar to the previously discussed studies. The higher dcp at burst onset implies that the propagation effects in the solar corona may become more significant with decreasing frequency, since the dcp value also decreases with frequency. Since Bursts 1 and 3 have higher dcp values than the other type III bursts and all bursts have different propagation directions, it seems that the significance of scattering of radio waves in

the corona may be dependent on the location, propagation direction and coronal conditions in the immediate vicinity of the radio source regions.

In the case of fundamental emission for the type III, there is a clear trend of the dcp increasing with frequency. This trend is only clear in the case of Bursts 3 and 6 for harmonic emission and an opposite trend is seen for Bursts 1 and 4. In the case of harmonic emission, an increase of dcp with frequency occurs due to the fact that the dcp of radio bursts is proportional to the strength of the coronal magnetic field, which decreases with height and thus with plasma frequency (Melrose, Dulk, and Gary, 1980; Mercier, 1990). The opposite trend in Bursts 1 and 4 cannot be explained by this relation with the magnetic field, and most likely there may still be some unaccounted leakage in Stoke U or V. The fundamental emission, on the other hand, is expected to be 100% circularly polarised, therefore the reason for the existence of such a trend in the fundamental emission is unclear. This trend in the fundamental was also reported with the MWA (Rahman, Cairns, and McCauley, 2020). Depolarisation within the source region has been suggested as a possible explanation (Wentzel, 1984). Rahman, Cairns, and McCauley (2020) show that beaming effects in the source region as a function of the magnetic-field strength, which in turn is dependent on the radial height, leads to the dcp to also decrease with height in the corona. In the case of the highly polarised Bursts 1 and 3, we find that the type III is highly circularly polarised during burst onset after which the dcp slowly decreases. In contrast, the Type I burst appears to have an almost constant dcp over each subband (Figure 5).

The most noteworthy finding is that all four type III bursts that occurred on 21 March 2019 within a time period of 30 minutes have a wide range of dcp values and one of these also shows an opposite sense of circular polarisation. This is explained by the fact that all of these bursts have different propagation directions. Strongly different source positions and propagation directions of subsequent type III radio bursts associated with the same eruptive event were also recently reported by Jebaraj et al. (2020). Different senses of circular polarisation within the same group or storm of type III bursts have previously been reported only in the case of type IIIs followed by type V bursts (Dulk, Gary, and Suzuki, 1980). Type V bursts represent continuum emission following a type III burst or group of type III bursts that can show an opposite sense of circular polarisation to the preceding type III bursts (Dulk, Gary, and Suzuki, 1980). However, recent observations of type V bursts with modern instrumentation have yet to be reported, which may have implications for the classification of these bursts as an entirely different type of bursts than type IIIs. Here we have shown that it is possible to have different senses of polarisation within the same storm of type III bursts. Despite the solar minimum conditions, multiple acceleration processes producing energetic electron beams occur in or in the vicinity of the two active regions that were present on the Sun that day. The active regions appear to be the source regions for the observed bursts. The type III and type I occurring on 8 April 2019 appear to have a similar source region, that is the active region on the eastern solar limb.

This study demonstrates for the first time LOFAR's spectropolarimetric imaging capabilities to investigate solar radio bursts. We used full Stokes parameters to estimate the correct degree of circular polarisation for the type I and type III bursts which occurred during March–April 2019. Our analysis shows that LOFAR is suitable to be used as a dynamic spectropolarimetric imaging instrument to study the radio emission from the Sun.

Data Availability The LOFAR datasets used in this analysis were obtained under project codes LC11_001 and LT10_002 and are available in the LOFAR Long Term Archive (LTA; https://lta.lofar.eu). The SWAP data is available from the Virtual Solar Observatory project (http://vso.nso.edu).

Declarations

Disclosure of Potential Conflicts of Interest The authors declare that they have no conflicts of interest.

References

Bastian, T.S., Benz, A.O., Gary, D.E.: 1998, Radio emission from solar flares. *Annu. Rev. Astron. Astrophys.* **36**, 131. DOI. ADS.

Benz, A.O., Zolliker, P.: 1985, Polarization of solar noise storm continuum and plasma wave density in the corona. *Astron. Astrophys.* **144**(1), 227. ADS.

Dulk, G.A.: 1985, Radio emission from the sun and stars. *Annu. Rev. Astron. Astrophys.* **23**, 169. DOI. ADS.

Dulk, G.A., Nelson, G.J.: 1973, The position of a type I storm source in the magnetic field of an active region. *Proc. Astron. Soc. Aust.* **2**(4), 211. DOI. ADS.

Dulk, G.A., Gary, D.E., Suzuki, S.: 1980, The position and polarization of type V solar bursts. *Astron. Astrophys.* **88**(1 – 2), 218. ADS.

Dulk, G.A., Suzuki, S.: 1980, The position and polarization of type III solar bursts. *Astron. Astrophys.* **88**(1 – 2), 203. ADS.

Dulk, G.A., Jacques, S., Smerd, S.F., MacQueen, R.M., Gosling, J.T., Steward, R.T., Sheridan, K.V., Robinson, R.D., Magun, A.: 1976, White light and radio studies of the coronal transient of 14 – 15 September 1973. I: material motions and magnetic field. *Solar Phys.* **49**, 369. ADS.

Elgarøy, E.Ø.: 1977, *Solar Noise Storms*. ADS.

Ellis, G.R.A.: 1969, Fine structure in the spectra of solar radio bursts. *Aust. J. Phys.* **22**, 177. DOI. ADS.

Ginzburg, V.L., Zhelezniakov, V.V.: 1958, On the possible mechanisms of sporadic solar radio emission (radiation in an isotropic plasma). *Soviet Astron.* **2**, 653. ADS.

Grognard, R.J.M., McLean, D.J.: 1973, Non-existence of linear polarization in type III solar bursts at 80 MHz. *Solar Phys.* **29**(1), 149. DOI. ADS.

Hales, C.A.: 2017, Calibration errors in interferometric radio polarimetry. *Astron. J.* **154**(2), 54. DOI. ADS.

Jebaraj, I.C., Magdalenić, J., Podladchikova, T., Scolini, C., Pomoell, J., Veronig, A.M., Dissauer, K., Krupar, V., Kilpua, E.K.J., Poedts, S.: 2020, Using radio triangulation to understand the origin of two subsequent type II radio bursts. *Astron. Astrophys.* **639**, A56. DOI. ADS.

Kai, K., Melrose, D.B., Suzuki, S.: 1985, In: McLean, D.J., Labrum, N.R. (eds.) *Storms*, 415. ADS.

Kathiravan, C., Ramesh, R., Nataraj, H.S.: 2007, The post-coronal mass ejection solar atmosphere and radio noise storm activity. *Astrophys. J. Lett.* **656**(1), L37. DOI. ADS.

Krupar, V., Maksimovic, M., Kontar, E.P., Zaslavsky, A., Santolik, O., Soucek, J., Kruparova, O., Eastwood, J.P., Szabo, A.: 2018, Interplanetary type III bursts and electron density fluctuations in the solar wind. *Astrophys. J.* **857**(2), 82. DOI.

Kumari, A., Ramesh, R., Kathiravan, C., Gopalswamy, N.: 2017a, New evidence for a coronal mass ejection-driven high frequency type II burst near the Sun. *Astrophys. J.* **843**, 10. DOI. ADS.

Kumari, A., Ramesh, R., Kathiravan, C., Wang, T.J.: 2017b, Strength of the solar coronal magnetic field - a comparison of independent estimates using contemporaneous radio and white-light observations. *Solar Phys.* **292**(11), 161. DOI. ADS.

Kumari, A., Ramesh, R., Kathiravan, C., Wang, T.J., Gopalswamy, N.: 2019, Direct estimates of the solar coronal magnetic field using contemporaneous extreme-ultraviolet, radio, and white-light observations. *Astrophys. J.* **881**(1), 24. DOI. ADS.

Kumari, A., Gireesh, G.V.S., Kathiravan, C., Mugundhan, V., Barve, I.V.: 2021, Solar radio spectro-polarimetry (50 – 500 MHz): design and development of cross-polarized log-periodic dipole antenna and configuration of receiver system. *arXiv e-prints*, arXiv. ADS.

Lin, R.P.: 1974, Non-relativistic solar electrons. *Space Sci. Rev.* **16**, 189. DOI. ADS.

Ma, Y., Xie, R.-x., Zheng, X.-m., Wang, M., Yi-hua, Y.: 2012, A statistical analysis of the type-III bursts in centimeter and decimeter wavebands. *Chin. Astron. Astrophys.* **36**, 175. DOI. ADS.

Maxwell, A., Swarup, G.: 1958, A new spectral characteristic in solar radio emission. *Nature* **181**, 36. DOI. ADS.

McCauley, P.I., Cairns, I.H., Morgan, J.: 2018, Densities probed by coronal type III radio burst imaging. *Solar Phys.* **293**(10), 132. DOI. ADS.

McCauley, P.I., Cairns, I.H., White, S.M., Mondal, S., Lenc, E., Morgan, J., Oberoi, D.: 2019, The low-frequency solar corona in circular polarization. *Solar Phys.* **294**(8), 106. DOI. ADS.

McCready, L., Pawsey, J.L., Payne-Scott, R.: 1947, Solar radiation at radio frequencies and its relation to sunspots. *Proc. Roy. Soc. London Ser. A, Math. Phys. Sci.* **190**(1022), 357.

Melrose, D.B.: 1975, Plasma emission due to isotropic fast electrons, and types I, II, and V solar radio bursts. *Solar Phys.* **43**, 211. DOI. ADS.

Melrose, D.B.: 1989, Depolarization of solar bursts due to scattering by low-frequency waves. *Solar Phys.* **119**(1), 143. DOI. ADS.

Melrose, D.B.: 2009, Coherent emission. In: Gopalswamy, N., Webb, D.F. (eds.) *Universal Heliophysical Processes*, *IAU Symposium* **257**, 305. DOI. ADS.

Melrose, D.B., Dulk, G.A., Gary, D.E.: 1980, Corrected formula for the polarization of second harmonic plasma emission. *Proc. Astron. Soc. Aust.* **4**(1), 50. ADS.

Melrose, D.B., Sy, W.N.: 1972, Plasma emission processes in a magnetoactive plasma. *Aust. J. Phys.* **25**, 387. DOI. ADS.

Mercier, C.: 1990, Polarisation of type-III bursts between 164-MHZ and 435-MHZ - structure and variation with frequency. *Solar Phys.* **130**(1 – 2), 119. DOI. ADS.

Morosan, D.E., Gallagher, P.T., Zucca, P., Fallows, R., Carley, E.P., Mann, G., et al.: 2014, LOFAR tied-array imaging of type III solar radio bursts. *Astron. Astrophys.* **568**, A67. DOI. ADS.

Morosan, D.E., Gallagher, P.T., Zucca, P., O'Flannagain, A., Fallows, R., Reid, H., et al.: 2015, LOFAR tied-array imaging and spectroscopy of solar S bursts. *Astron. Astrophys.* **580**, A65. DOI. ADS.

Morosan, D.E., Gallagher, P.T., Fallows, R.A., Reid, H., Mann, G., Bisi, M.M., Magdalenić, J., et al.: 2017, The association of a J-burst with a solar jet. *Astron. Astrophys.* **606**, A81. DOI. ADS.

Morosan, D.E., Carley, E.P., Hayes, L.A., Murray, S.A., Zucca, P., Fallows, R.A., McCauley, J., Kilpua, E.K.J., Mann, G., Vocks, C., Gallagher, P.T.: 2019, Multiple regions of shock-accelerated particles during a solar coronal mass ejection. *Nat. Astron.* **3**, 452. DOI. ADS.

Mugundhan, V., Ramesh, R., Kathiravan, C., Gireesh, G.V.S., Hegde, A.: 2018a, Spectropolarimetric observations of solar noise storms at low frequencies. *Solar Phys.* **293**(3), 41. DOI. ADS.

Mugundhan, V., Ramesh, R., Kathiravan, C., Gireesh, G.V.S., Kumari, A., Hariharan, K., Barve, I.V.: 2018b, The first low-frequency radio observations of the solar corona on ≈200 km long interferometer baseline. *Astrophys. J. Lett.* **855**(1), L8. DOI. ADS.

Payne-Scott, R.: 1949, Bursts of solar radiation at metre wavelengths. *Aust. J. Sci. Res., Ser. A Phys. Sci.* **2**, 214. DOI. ADS.

Rahman, M.M., Cairns, I.H., McCauley, P.I.: 2020, Spectropolarimetric imaging of metric type III solar radio bursts. *Solar Phys.* **295**(3), 51. DOI. ADS.

Ramesh, R., Mugundhan, V., Prabhu, K.: 2020, New evidence for spatio-temporal fragmentation in the solar flare energy release. *Astrophys. J. Lett.* **889**(1), L25. DOI. ADS.

Ramesh, R., Kathiravan, C., Sundararajan, M.S., Barve, I.V., Sastry, C.V.: 2008, A low-frequency (30 – 110 MHz) antenna system for observations of polarized radio emission from the solar corona. *Solar Phys.* **253**(1 – 2), 319. DOI. ADS.

Ramesh, R., Sasikumar Raja, K., Kathiravan, C., Narayanan, A.S.: 2013, Low-frequency radio observations of picoflare category energy releases in the solar atmosphere. *Astrophys. J.* **762**(2), 89. DOI. ADS.

Reid, H.A.S., Kontar, E.P.: 2017, Imaging spectroscopy of type U and J solar radio bursts with LOFAR. *Astron. Astrophys.* **606**, A141. DOI. ADS.

Reid, H.A.S., Ratcliffe, H.: 2014, A review of solar type III radio bursts. *Res. Astron. Astrophys.* **14**(7), 773. DOI. ADS.

Reiner, M.J., Fainberg, J., Stone, R.G.: 1995, Large-scale interplanetary magnetic field configuration revealed by solar radio bursts. *Science* **270**, 461. DOI. ADS.

Robinson, R.D.: 1983, Scattering of radio waves in the solar corona. *Proc. Astron. Soc. Aust.* **5**(2), 208. DOI. ADS.

Robishaw, T., Heiles, C.: 2021, In: Wolszczan, A. (ed.) *The Measurement of Polarization in Radio Astronomy*, 127. DOI. ADS.

Saint-Hilaire, P., Vilmer, N., Kerdraon, A.: 2013, A decade of solar type III radio bursts observed by the Nançay radioheliograph 1998 – 2008. *Astrophys. J.* **762**, 60. DOI. ADS.

Santandrea, S., Gantois, K., Strauch, K., Teston, F., Tilmans, E., Baijot, C., Gerrits, D., De Groof, A., Schwehm, G., Zender, J.: 2013, PROBA2: mission and spacecraft overview. *Solar Phys.* **286**(1), 5. DOI. ADS.

Sasikumar Raja, K., Kathiravan, C., Ramesh, R., Rajalingam, M., Barve, I.V.: 2013, Design and performance of a low-frequency cross-polarized log-periodic dipole antenna. *Astrophys. J. Suppl.* **207**(1), 2. DOI. ADS.

Sastry, C.V.: 2009, Polarization of the thermal radio emission from outer solar corona. *Astrophys. J.* **697**(2), 1934. DOI. ADS.

Seaton, D.B., Berghmans, D., Nicula, B., Halain, J.-P., De Groof, A., Thibert, T., Bloomfield, D.S., Raftery, C.L., Gallagher, P.T., Auchère, F., Defise, J.-M., D'Huys, E., Lecat, J.-H., Mazy, E., Rochus, P., Rossi, L., Schühle, U., Slemzin, V., Yalim, M.S., Zender, J.: 2013, The SWAP EUV imaging telescope part I: instrument overview and pre-flight testing. *Solar Phys.* **286**, 43. DOI. ADS.

Spicer, D.S., Benz, A.O., Huba, J.D.: 1982, Solar type I noise storms and newly emerging magnetic flux. *Astron. Astrophys.* **105**(2), 221. ADS.

Stappers, B.W., Hessels, J.W.T., Alexov, A., Anderson, K., Coenen, T., Hassall, T., et al.: 2011, Observing pulsars and fast transients with LOFAR. *Astron. Astrophys.* **530**, A80. DOI. ADS.

Stewart, R.T., Labrum, N.R.: 1972, Meter-wavelength observations of the solar radio burst storm of August 17 22, 1968. *Solar Phys.* **27**(1), 192. DOI. ADS.

Stone, R.G., Fainberg, J.: 1971, A U-type solar radio burst originating in the outer corona. *Solar Phys.* **20**, 106. DOI. ADS.

Suzuki, S., Dulk, G.A.: 1985, In: McLean, D.J., Labrum, N.R. (eds.) *Bursts of Type III and Type V.*, 289. ADS.

Swarup, G., Stone, P.H., Maxwell, A.: 1960, The association of solar radio bursts with flares and prominences. *Astrophys. J.* **131**, 725. DOI. ADS.

Takakura, T.: 1963, Origin of solar radio type I bursts. *Publ. Astron. Soc. Japan* **15**, 462.

Thejappa, G., Kundu, M.R.: 1991, New observations of solar noise storm radiation at decameter wavelengths. *Solar Phys.* **132**(1), 155. DOI. ADS.

Tingay, S.J., Goeke, R., Bowman, J.D., Emrich, D., Ord, S.M., Mitchell, D.A., Morales, M.F., Booler, T., et al.: 2013, The Murchison widefield array: the square kilometre array precursor at low radio frequencies. *Publ. Astron. Soc. Aust.* **30**, e007. DOI. ADS.

van Haarlem , M.P., Wise, M.W., Gunst, A.W., Heald, G., McKean, J.P., Hessels, J.W.T., et al.: 2013, LOFAR: the LOw-Frequency ARray. *Astron. Astrophys.* **556**, A2. DOI. ADS.

Wentzel, D.G.: 1984, Polarization of fundamental type-III radio bursts. *Solar Phys.* **90**(1), 139. DOI. ADS.

Wild, J.P.: 1950, Observations of the spectrum of high-intensity solar radiation at metre wavelengths. III. Isolated bursts. *Aust. J. Sci. Res., Ser. A Phys. Sci.* **3**, 541. ADS.

Wild, J.P.: 1951, Observations of the spectrum of high-intensity solar radiation at metre wavelengths. IV. Enhanced radiation. *Aust. J. Sci. Res., Ser. A Phys. Sci.* **4**, 36. DOI. ADS.

Wild, J.P.: 1963, The radio emission of the Sun, In: *Radiotekhnika* **1**. ADS.

Wild, J.P.: 1967, The radioheliograph and the radio astronomy programme of the Culgoora observatory. *Proc. Astron. Soc. Aust.* **1**, 38. ADS.

Yu, S., Chen, B., Bastian, T., Gary, D.E.: 2019, Imaging spectroscopic observations of type I noise storms with ultrahigh temporal and spectral resolution. In: *AGU Fall Meeting Abstracts* **2019**, SH23C. ADS.